Cobalt/nitrogen doped porous carbon as catalysts for efficient oxygen reduction reaction: towards hybrid enzymatic biofuel cells

Feng, Xiaogeng; Xiao, Xinxin; Zhang, Jingdong; Guo, Liping; Xiong, Ying

Published in:
Electrochimica Acta

Link to article, DOI:
10.1016/j.electacta.2021.138791

Publication date:
2021

Document Version
Peer reviewed version

Cobalt/nitrogen doped porous carbon as catalysts for efficient oxygen reduction reaction: towards hybrid enzymatic biofuel cells

Xiaogeng Feng , Xinxin Xiao , Jingdong Zhang , Liping Guo , Ying Xiong

PII: S0013-4686(21)01081-1
DOI: https://doi.org/10.1016/j.electacta.2021.138791
Reference: EA 138791

To appear in: *Electrochimica Acta*

Received date: 18 March 2021
Revised date: 13 May 2021
Accepted date: 12 June 2021

Please cite this article as: Xiaogeng Feng , Xinxin Xiao , Jingdong Zhang , Liping Guo , Ying Xiong , Cobalt/nitrogen doped porous carbon as catalysts for efficient oxygen reduction reaction: towards hybrid enzymatic biofuel cells, *Electrochimica Acta* (2021), doi: https://doi.org/10.1016/j.electacta.2021.138791

Cobalt/nitrogen doped porous carbon as catalysts for efficient oxygen reduction reaction: towards hybrid enzymatic biofuel cells

Xiaogeng Feng[a], Xinxin Xiao[b*], Jingdong Zhang[b], Liping Guo[c] and Ying Xiong[a*]

[a]College of Chemistry, Key Laboratory of Rare-scattered Elements of Liaoning Province, Liaoning University, Shenyang 110036, PR China

[b]Department of Chemistry, Technical University of Denmark, Kongens Lyngby 2800, Denmark

[c]College of Chemistry, Key Laboratory of Nanobiosensing and Nanobioanalysis at Universities of Jilin Province, Northeast Normal University, Changchun, 130024, PR China

[*]Corresponding authors.

E-mail: xixiao@kemi.dtu.dk (X. Xiao), xiongying_1977@hotmail.com (Y. Xiong)

Abstract

Electrochemical oxygen reduction reaction (ORR) represents a crucial cathodic process of different fuel cells. The development of highly active and stable noble metal-free ORR electrocatalysts remains as one of major challenges. Herein, we report cobalt/nitrogen co-doped porous carbon materials (Co-N-C) from well-designed bimetal-organic frameworks (Zn_xCo_{100-x}-ZIF) as efficient ORR electrocatalysts in both pH-neutral and alkaline solutions. The compositional and structural features, and the corresponding ORR activity can be tailored by tuning the Zn/Co ratio in the precursor. Remarkable features of large surface-area and suitable graphitization degree and well-dispersed Co-N-C moieties, enable a high catalytic efficiency. The optimized electrocatalyst registers considerable ORR performance with a high half-wave potential of 0.65 V vs RHE and a saturated current density of 5.30 mA cm^{-2} close to the value of the commercial Pt/C in 0.1 M pH 7.0 PBS, and considerable operational stability and tolerance to glucose. A preliminary one-compartment hybrid glucose/O_2 enzymatic biofuel cell, consisting of Co-N-C-10 abiotic cathode and glucose oxidising bioanode, is constructed and tested. Furthermore, Co-N-C also presents reasonable ORR electrocatalytic activity and operational stability in alkaline condition.

Keywords： Cobalt and nitrogen-doped porous carbon; Oxygen reduction reaction; Neutral solution; Metal-organic frameworks; Electron transfer

Introduction

Electrochemical oxygen reduction reaction (ORR) is the most significant cathodic reaction of fuel cells [1, 2]. Pt-based materials have been identified as the most excellent catalysts toward ORR in acidic conditions. However, crucial challenges, including the high costs, scarcity, poor durability and possible methanol crossover, still remain [3, 4]. Alternatively, the preparation of nonprecious alternatives, such as earth-abundant metal based materials (*e.g.*, alloys, oxides) and metal-free carbons materials, is thus an active research area [5-7]. Recently, transition metal nitrogen carbon (M-N-C) composites, such as Co-N-C, have been identified as one of the most attractive ORR catalysts attributed to their low price, great catalytic activity and considerable stability [8, 9]. It's noteworthy that many reported M-N-C materials suffer from the tedious preparation process and uncontrolled structure and composition [10]. Therefore, it is imperative to establish an easy and controlled strategy for M-N-C materials with attractive characters.

Meanwhile, biofuel cells (EBFCs) are a subclass of electrochemical device utilizing enzymatic catalysts to harvest electricity from the chemical energy in biofuels [11]. Due to the intrinsic properties of the enzyme, EBFCs typically operates at a mild pH between 5 and 8. EBFCs hold the promise to activate implantable and wearable medical devices [12-14]. Bilirubin oxidase (BOx) [15-19], a type of blue copper enzyme, is a typical enzyme used for ORR at the biocathode, outperforming Pt with a lower ORR overpotential at neutral pH [20]. However, the BOx modified bioelectrodes suffer from significantly poorer operational stability in comparison to Pt. Irreversible deactivation of the oxidised Cu atoms of BOx [21] and the inhibition by

F^- [22] and urate *etc*. are problematic. Alternatively, using abiotic and non-noble metal based ORR catalysts that are more robust and tolerant to inhibitors is promising for a hybrid EBFC [23], *i.e.* a cell consisting of an enzymatic bioanode and an abiotic cathode, similar to that in a hybrid microbial fuel cell [24-26]. Atanassov *et al.* have explored a large group of Pt-free catalysts for ORR in neutral pH [27-29].

Metal-organic frameworks (MOFs), made of metal ions with coordinative organic ligands, show attractive features including considerably large surface-area, high porosity, tuneable structure and composition [30-32]. Zeolitic imidazolate frameworks (ZIFs), including ZIF-67 and ZIF-8, have been reported to be good precursors for the preparation of M-N-C catalysts, featuring the abundant carbon and nitrogen ligands, and uniform spatial distribution of metal ion [33, 34]. Among them, ZIF-8 can be annealed to generate amorphous carbon materials enjoying large surface area and rich N content, but with limited satisfying graphitization degree [35, 36]. Meanwhile, ZIF-67 derived Co doped carbon materials exhibit favorable electronic conductivity but lower surface area in comparison to ZIF-8 [37, 38]. Thus, the rational combination of ZIF-8/ZIF-67 based precursors will lead to the bimetallic ZIF-templated porous carbons enjoying large surface area, increased graphitization, and widely isolated Co-N_x moieties.

In the present contribution, we prepare a range of cobalt and nitrogen doped porous carbon catalysts (Co-N-C) through a simple pyrolysis of bimetal-organic frameworks (Zn_xCo_{100-x}-ZIF) with various Zn/Co ratios (**Scheme 1**). During pyrolysis, the evaporative Zn could enable the resulting Co-N-C with enhanced porosity and

surface area. Adjusting the original Zn/Co ratio in precursor offers an opportunity for the optimization of effective surface area, porosity, Co content and graphitization degree, and thus the corresponding ORR activity of Co-N-C materials. Remarkably, the optimized Co-N-C exhibits excellent ORR performance *via* a four-electron pathway, in comparable to commercial Pt/C in neutral solution. Preliminary results demonstrate the feasibility of the proposed abiotic cathode for a membrane-less glucose/O_2 EBFC in neutral pH. To the best of our knowledge, there are only few reports in such a membrane-less hybrid EBFC [23].

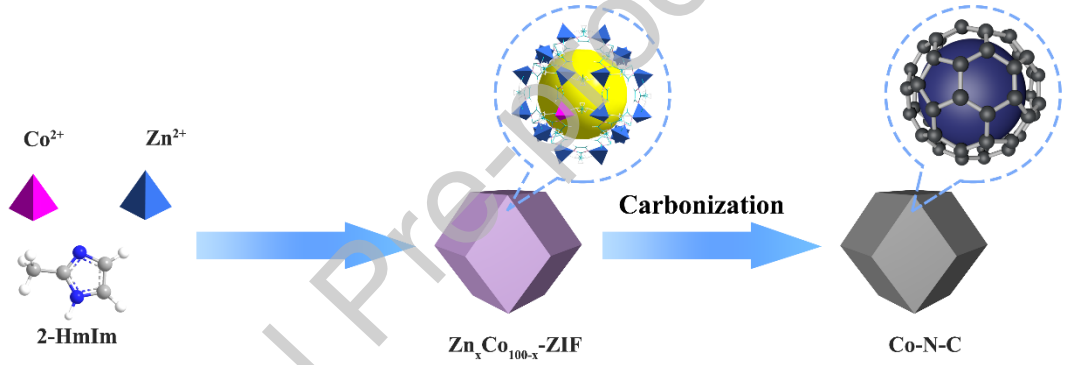

Scheme 1 Illustration of the synthesis of Co-N-C.

Experimental

1. Reagents and apparatus

$Co(NO_3)_2 \cdot 6H_2O$ (99%), $Zn(NO_3)_2 \cdot 6H_2O$ (99%), Nafion solution (5 wt%), 2-methylimidazole (Hmim, 98%) and KOH (85%) were obtained from Aladdin. N_2 and O_2 were from Shenyang Shuntai Special Gas Co., Ltd.

Scanning electron microscopy (SEM, Hitachi S-4800) equipped with the energy dispersive X-ray (EDX) detector was used for morphology and elemental characterization. Transmission electron microscopy (TEM) was performed on FEI

Tecnai G2 F20 electron microscope operated at 200 kV. X-ray diffraction (XRD, Bruker diffractometer D8 ADVANCE, Germany) patterns and X-ray photoelectron spectroscopy (XPS, ESCA LAB spectrometer, USA; a monochromatic Al K_α source) were used to analyse the material composition. Brunauer-Emmett-Teller (BET) method was adopted to determine the specific surface area and the pore size distribution. Raman spectra were acquired with a confocal microprobe Raman system (HR800, JobinYvon, 532 nm).

2. Catalyst synthesis

2.1 Synthesis of ZIF-8 nanocrystals.

The ZIF-8 nanocrystals were obtained following the previous report with some modifications [39]. Briefly, $Zn(NO_3)_2 \cdot 6H_2O$ (3.36 g) and Hmim (7.40 g) were added into 160 mL methanol (MeOH), respectively. The above aqueous solutions were then blended with stirring in a course of 24 h at room temperature, with the product collected with centrifugation and washing with MeOH, allowed to be dried overnight at 60℃.

2.2 Synthesis of ZIF-67 nanocrystals.

The ZIF-67 nanocrystals were prepared by following a lightly modified report [40]. 20 mL aqueous solution of Hmim (5.5 g) was added into 6 mL $Co(NO_3)_2 \cdot 6H_2O$ (0.90 g) aqueous solution, under vigorous stirring for 24 h, leading to purple precipitates. The products were then collected by centrifugation, washed with H_2O for three times, and dried at 60℃ overnight.

2.3 Synthesis of bimetallic ZIF nanocrystals.

First, $Zn(NO_3)_2 \cdot 6H_2O$ was mixed with $Co(NO_3)_2 \cdot 6H_2O$ in various molar ratios of Zn^{2+}/Co^{2+} (19:1, 9:1, 4:1, 3:2) and dissolved in 160 mL MeOH, into which 160 mL Hmim (7.40 g) methanolic solution was added, stirring for reaction over 24 h. The final product was collected with subsequent centrifugation, MeOH washing and drying at 60℃ overnight.

2.4 Preparation of cobalt/nitrogen-doped porous carbon materials.

The as-produced bimetallic ZIF were annealed in a tube furnace (temperature: 910 ℃; duration: 3 h; heating rate: 2 ℃ min^{-1}) under flowing N_2 atmosphere.

3. Electrochemical characterization methods

Linear sweep voltammetry (LSV, scan rate: 5 mV s^{-1}) measurements were performed with a CHI 730E electrochemical workstation in 0.1 M pH 7.0 phosphate buffer solution (PBS) or 0.1 M KOH, with a rotating disk electrode (RDE)/rotating ring-disk electrode (RRDE) working electrode, a carbon rod counter electrode and a Ag/AgCl reference electrode (saturated KCl). 3 mg catalyst powders were dispersed in 1 mL 0.5 wt% Nafion aqueous solution with ultrasonication, with 20 μL of the ink casting onto a well-polished glassy carbon electrode (GCE, 0.19625 cm^{-2}) and dried at room temperature, leading to the working electrode. All reported potentials, unless stated otherwise, were against the reversible hydrogen electrode (RHE) (E_{RHE} = $E_{Ag/AgCl}$ + 0.197 + 0.059 pH). In prior to ORR experiment, O_2 was used to bubble the electrolyte for no less than 0.5 h and maintained in the headspace of the electrochemical cell throughout the test.

The ORR associated number of electrons (n) transferred is determined by

Koutecky-Levich equation [41]:

$$\frac{1}{j} = \frac{1}{j_k} + \frac{1}{j_l} = \frac{1}{j_k} + \frac{1}{B\omega^{\frac{1}{2}}} \quad (1)$$

$$B = 0.2nFC_O D_O^{\frac{2}{3}} \upsilon^{-\frac{1}{6}} \quad (2)$$

where j, j_k and j_l are the measured, kinetic and diffusion-limiting current densities, respectively, ω is the rotation speed in rpm, F represents the Faraday constant (96485 C mol^{-1}), C_o is the bulk O_2 concentration (1.2×10^{-6} mol cm^{-3}), D_o is the diffusion coefficient of O_2 (1.9×10^{-5} cm^2 s^{-1}), υ is the kinetic viscosity of the electrolyte (0.01 cm^2 s^{-1}).

RRDE experiments (1600 rpm) were carried out on a ring-disk electrode with a scan rate of 5 mV s^{-1} for the disk electrode, while the working potential of ring electrode was held constantly at 1.4 V *vs.* RHE.

In the RRDE measurements, the number of electrons transferred (n) and peroxide percentage can be calculated via [42]:

$$n = \frac{4 \times I_d}{I_d + \frac{I_r}{N}} \quad (3)$$

$$HO_2^- \% = \frac{200 \times I_r}{I_d \times N + I_r} \quad (4)$$

where I_d and I_r represent the disk and ring currents, respectively, N indicates the collection efficiency (0.37).

4. A hybrid glucose/O_2 biofuel cell construction and measurement

A GOx bioanode on a pre-polished GCE was obtained by following our well-established procedure [43, 44]. Osmium complex modified redox polymer $[Os(2,2'\text{-bipyridine})_2(polyvinylimidazole)_{10}Cl]^{+/2+}$ ($Os(bpy)_2PVI$) was used as the redox mediator of GOx. The GOx bioanode and the cobalt/nitrogen-doped porous

carbon based abiotic cathode were assembled as a membrane-less EBFC and tested in air-equilibrated 0.1 M pH 7.0 PBS with 5 mM glucose at room temperature. LSVs at 1 mV s^{-1} were measured to generate polarization curves.

Results and discussion

1. Catalysts structure and composition

Bimetallic ZIF with a range of Zn/Co molar ratios has been fabricated and well characterized in terms of composition and morphology. The XRD patterns of Zn_xCo_{100-x}-ZIF (**Figure S1**) match well with ZIF-8 and ZIF-67 showing identical crystalline features [33]. SEM images (**Figure 1A** and **Figure S2**) display that, as the Zn/Co molar ratio decreases, the well- defined Zn_xCo_{100-x}-ZIF nanocrystals in a dodecahedral shape with size gradually increases from ~90 to ~210 nm. The rough sizes of particles for these samples are ~90, ~ 100, ~ 110, ~ 120, ~ 150 and ~210 nm for Zn_xCo_{100-x}-ZIF (x=0, 5, 10, 20, 40 and 100), respectively. Subsequently, a series of Co-N-C materials with different Co contents are synthesized through the carbonization of Zn_xCo_{100-x}-ZIF in N_2 atmosphere at 910℃ for a period of 3 h. The evaporation of Zn during annealing leads to mesopores structure and thus increased surface area. Co-N-C materials inherit the polyhedral morphology from their precursors, without significantly structural collapse (**Figure 1B** and **Figure S3**). The corresponding size decreases by about 30 nm for these samples which are ~ 60, ~ 75, ~ 80, ~ 90, ~ 115 and ~195 nm for N-C and Co-N-C-x (x=5, 10, 20, 40 and 100), respectively, due to the decomposition and shrinkage during pyrolysis process. It can be seen in TEM images that Co-N-C-10 presents the symmetric dodecahedral

framework (**Figure S4A**). The EDX spectra (**Figure 1C)** display the signals for Co, N, C and O elements without the presence of Zn element, confirming the formation of Co-N-C and the evaporation of Zn. The element O is likely from surface oxidation. The EDX mapping (**Figure 1D-G** and **Figure S4B-F**) shows the homogenously spatial distribution of C, Co, and N element in the resulting Co-N-C materials.

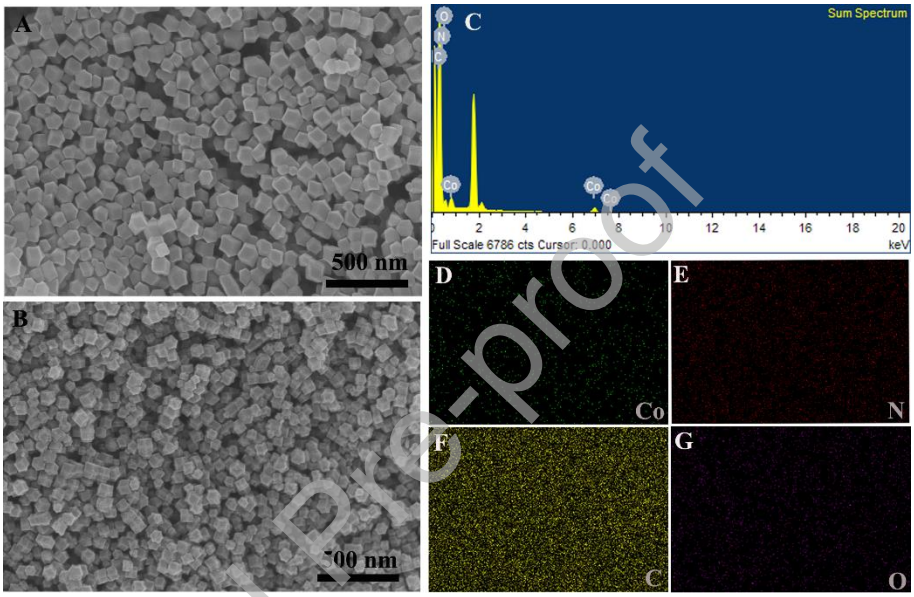

Figure 1 SEM images of (A) $Zn_{90}Co_{10}$-ZIF and (B) Co-N-C-10. (C) EDX spectrum and (D-G) elemental mapping of Co-N-C-10.

The XRD patterns further demonstrate the complete conversion of bimetallic ZIF into Co, N-doped porous carbon after carbonization (**Figure 2A**). Carbon is found in the resulting materials, with two peaks at ca. 25° and 44° attributed to its (002) and (101) planes, respectively. The broad peak at around 25° shifts positively and becomes relatively sharper with increasing Co content, suggesting the improved graphitization. This conclusion is further validated by the declined I_D/I_G ratio in Raman spectra (**Figure 2B**). The higher Co/Zn ratio in Zn_xCo_{100-x}-ZIF leads to the

enhanced graphitization of resultant Co-N-C materials at the same pyrolysis condition, because of the catalytic Co. The presence of metallic face-centred cubic (fcc) Co (JCPDS 15-0806), generated from the reduction of carbon for Zn_xCo_{100-x}-ZIF, is confirmed by XRD, with peaks at around 44.2°, 51.5° and 75.8° associated with the (111), (200) and (220) planes, respectively. Nitrogen adsorption was performed to investigate the pore features of Co-N-C materials at 77 K. The Co-N-C materials (**Figure S5A**) display a classic type-Ⅳ isotherm showing an H4-type hysteresis loop, indicative of the existence of both micr-/meso-pores. Furthermore, the pore size distribution plot in **Figure S5B** reveals that all samples show a narrow size distribution of micropore, located at ~ 1.4 nm and numerous mesopores. The Brunner-Emmet-Teller (BET) surface areas are 570.4, 538.2, 468.8, 412.5, 377.9, and 223.6 m^2 g^{-1} for N-C and Co-N-C-x (x= 5, 10, 20, 40 and 100), respectively, comparable to published reports of MOFs-derived M-N-C materials [45-49]. These results manifest that that manipulation the Zn/Co ratio in the precursor without tedious processes could adjust the specific surface area of Co-N-C. The accessibility of active sites and the diffusion of dissolved dioxygen can be improved by the manipulated large surface area. XPS displays the existence of C, Co, N and O species (**Figure 2C**), matching the observation from the EDX mapping results. Co 2p XPS spectrum displays two spin-orbit doublets and their corresponding satellite peaks (**Figure 2D**). The Co $2p_{3/2}$ and $2p_{1/2}$ peaks are further split into subpeaks of Co^0 (778.3 and 793.6 eV), Co^{3+} (780.4 and 796.3 eV) and Co^{2+} (782.2 and 798.8 eV). The appearance of Co^{2+} and Co^{3+} could be originated from the partial oxidation of metallic

Co surface in air. In N 1s XPS spectrum, five groups of nitrogen species can be identified, including pyridinic type N (398.3 eV), Co-N_x (399.1 eV), pyrrolic type N (400.7 eV), graphitic type N (402.1 eV), and oxidized type N (404.7 eV) (**Figure 2E**), with all N species involved in the ORR besides the oxidized-N [47, 50].

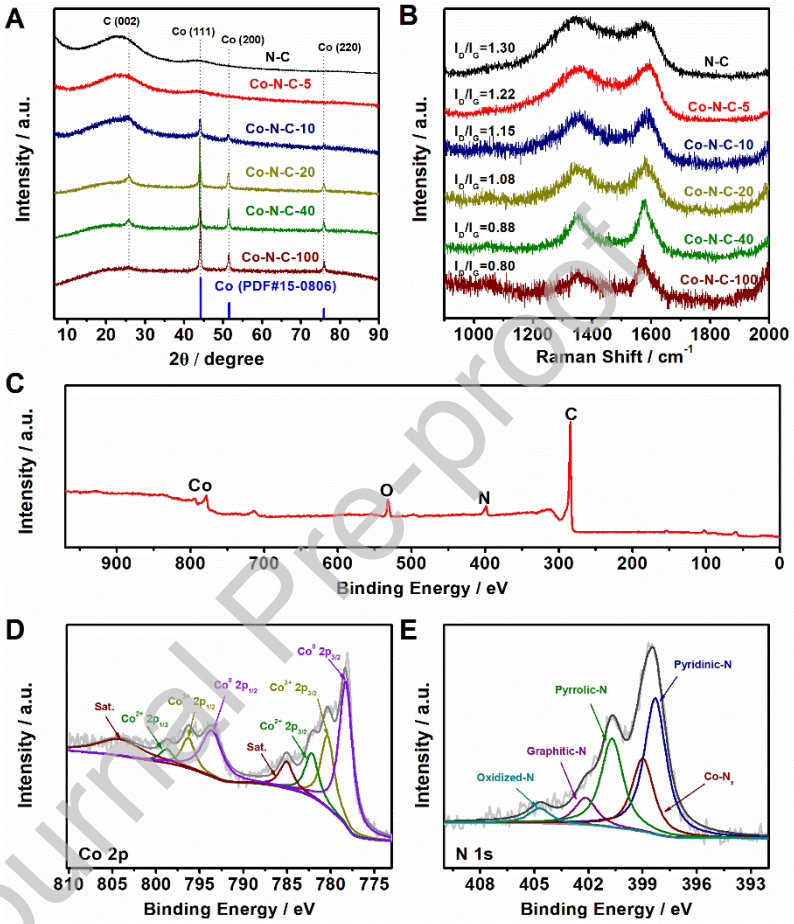

Figure 2 (A) XRD patterns and (B) Raman spectra of N-C, Co-N-C-5, Co-N-C-10, Co-N-C-20, Co-N-C-40 and Co-N-C-100. (C) The survey XPS spectrum and detailed XPS spectra of (D) Co 2p and (E) N 1s of Co-N-C-10.

2. Electrocatalytic activity and durability toward ORR in neutral solution

The ORR performance of the Co-N-C samples are investigated by LSV on a RDE in O_2-saturated 0.1 M pH 7.0 PBS. As shown in **Figure 3A** and **B**, Co-N-C-100 and N-C exhibit relatively poor ORR activity. Remarkably, among all the Co-N-Cs prepared in this study, Co-N-C-10 exhibits the best ORR activity, with a positive half-wave potential ($E_{1/2}$) of 0.65 V vs. RHE and a high diffusion-limiting current density (J_L) of 5.30 mA cm^{-2} at 0 V vs. RHE, very close to those of commercial 20 wt % Pt/C (0.70 V vs. RHE, 5.37 mA cm^{-2}). The onset potential (E_{Onset}) is determined to be 0.90 V vs. RHE for Co-N-C-10 and 0.94 V vs. RHE for Pt/C, respectively, although lower than the formal redox potential of the CuT1 of BOx (1.08 V vs. RHE [15, 51]), one of the most common ORR enzymes used for EBFCs [15]. The comparable $E_{1/2}$ and J_L of Co-N-C-10 catalyst demonstrates its rapid kinetics for ORR. Because of the presence of Co, the graphitization degree of carbon is greatly improved, confirmed by XRD and Raman analysis (**Figure 2A and 2B**). The graphitic carbon is an important component to achieve the good ORR activity due to its fast electron transfer and high conductivity [52, 53]. Meanwhile, the active site is directly associated with the Co-N-C moieties to adsorb and catalyze oxygen reduction [53, 54]. On the other hand, nitrogen dopants with the lone pair electron could induce structural and electronic alterations on the neighbour carbon atoms, that can increase the turnover of the adsorption and activation of molecular oxygen, thus allowing accelerated overall ORR process [55, 56]. Moreover, the large specific surface areas resulting from the

evaporation of Zn during pyrolysis can expose more active sites. All these factors, including large surface area, porosity, optimized graphitization degree and abundant Co-N-C moieties, are likely to synergistically contribute to the superior ORR activity of Co-N-C-10 catalyst. Actually, the Co-N-C-10 also registers excellent ORR performance in comparison to the other non-nobel metal based ORR catalysts (**Table S1**).

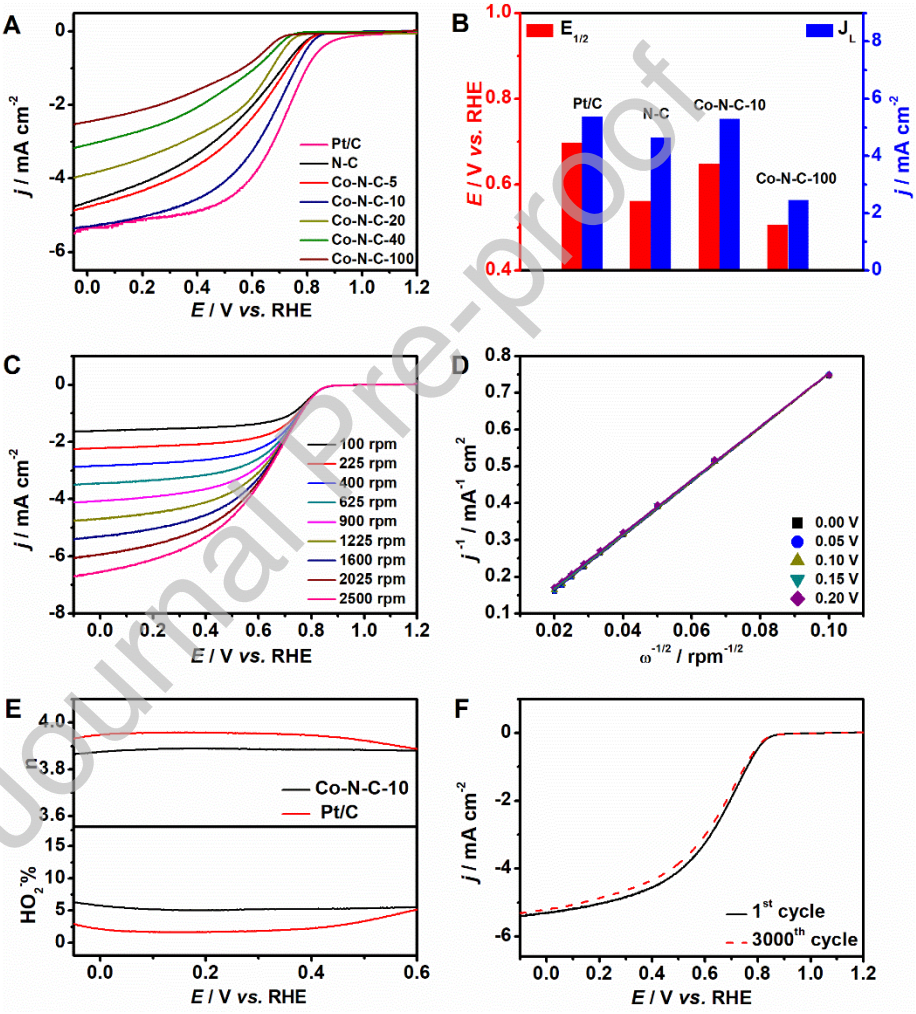

Figure 3 (A) LSVs of NC, Co-N-C-5, Co-N-C-10, Co-N-C-20, Co-N-C-40, Co-N-C-100 and commercial Pt/C catalyst in O_2-saturated 0.1 M pH 7.0 PBS at 1600 rpm; Scan rate: 5 mV s^{-1}. (B) Comparison of $E_{1/2}$ and J_L for N-C, Co-N-C-10,

Co-N-C-100 and commercial Pt/C catalysts. (C) LSVs of Co-N-C-10 at different rotation speeds; Scan rate: 5 mV s^{-1}. (D) Koutecky-Levich plots of Co-N-C-10 generated from the LSVs in (C) at various potentials. (E) HO_2^- yields and number of electrons transferred (n) of Co-N-C-10 and Pt/C calculated from RRDE. (F) LSVs of Co-N-C-10 before and after 3000 cycles continuous CV sweeps; Scan rate: 5 mV s^{-1}.

ORR kinetics of the Co-N-C-10 sample and other counterparts are further evaluated by RDE at various rotating speeds in a range of 100 to 2500 rpm (**Figure 3C**). The limiting cathodic current density rises with rotating speed, indicative of the enhanced mass transport of dioxygen from the bulk electrolyte to the Co-N-C-10 surface. The good linearity of the Koutecky-Levich (K-L) plots (**Figure 3D**) suggests similar number of electrons transferred (n) at various potentials ranging from 0 to 0.2 V vs. RHE. The value of n is calculated to be ~3.88 based on the K-L plots, illustrating Co-N-C-10 favors a $4e^-$ ORR pathway, close to the benchmark Pt/C catalyst (~3.94, **Figure S6**). In contrast, the other as-prepared samples register rather smaller n of ~3.60 for N-C, ~3.69 for Co-N-C-5, ~3.46 for Co-N-C-20, ~3.02 for Co-N-C-40, and ~2.87 for Co-N-C-100, respectively (**Figure S7-S11**).

To further quantify the yield of HO_2^- in the process of ORR, RRDE technique is applied to test the Co-N-C-10 and Pt/C catalyst (**Figure 3E**). The HO_2^- yield of Co-N-C-10 is below 10% and the value of n is in a range of 3.87-3.89 between -0.05 and 0.60 V vs. RHE, comparable to those of Pt/C and in agreement of the observations of the RDE derived K-L plots (**Figure 3D**). These results demonstrate

that the ORR process catalysed by Co-N-C-10 prefers a four-electron pathway, as effective as that on commercial Pt/C.

The long-term operational stability of the catalysts is another crucial parameter. Co-N-C-10 remains high durability with little variation in LSV curves after 3000 continuous CV cycles in a course of 25 h (**Figure 3F**). Such a stability outperforms the enzymatic biocathode counterparts, which generally exhibit a half-life time in several hours [11, 15] under continuous operation due to the fragile nature of enzymes. After long-term stability test, the Co-N-C-10 catalyst has been further analyzed by TEM and XPS. It is found in TEM images (**Figure** S**12**A and **B**) that the Co-N-C-10 still maintains its original structure and morphology. The XPS of Co-N-C-10 after the 3000 continuous CV cycles exhibits that the fraction of Co^0 has an obvious decrease and the content of Co-O phase increases (**Figure S12C** and **D**), indicative of the oxidation of metal Co.

Regarding to the selectivity, which is an issue for Pt based catalysts [57, 58], the presence of 20 mM glucose poses little effect upon the onset potential of Co-N-C-10, causing a slight decrease of the ORR current density (**Figure S13**). Given its excellent selectivity towards ORR, Co-N-C-10 based cathode can be directly assembled with a GCE/$Os(bpy)_2$PVI/GOx bioanode for a hybrid EBFC without using separative membranes (**Figure 4A**). In air-equilibrated 0.1 M pH 7.0 PBS with 5 mM glucose, the resultant hybrid EBFC registers a maximum power density (P_{max}) of 3.9 μW cm^{-2} at 0.087 V, an open circuit voltage (OCV) of 0.335 V and a short-circuit current density of 74 μA cm^{-2} (**Figure 4B**). Although the P_{max} of the hybrid EBFC here

doesn't reach 1 mW cm^{-2} [11] and the OCV is far below the theoretical value of 1.18 V of a glucose/O_2 fuel cell undergoing $2e^-$ involved glucose oxidation at standard conditions [11], the results here demonstrate the feasibility of the abiotic cathode for membrane-less hybrid EBFC. The current collector used here is GCE, which can be replaced with porous carbon electrode featuring high-surface-area to improve the output power density [59, 60]. The delivered OCV can be enhanced by reducing the overpotentials of the anode/cathode, especially the bioanode here can be replaced with a glucose dehydrogenase [23] with a much negative onset potential for glucose oxidation.

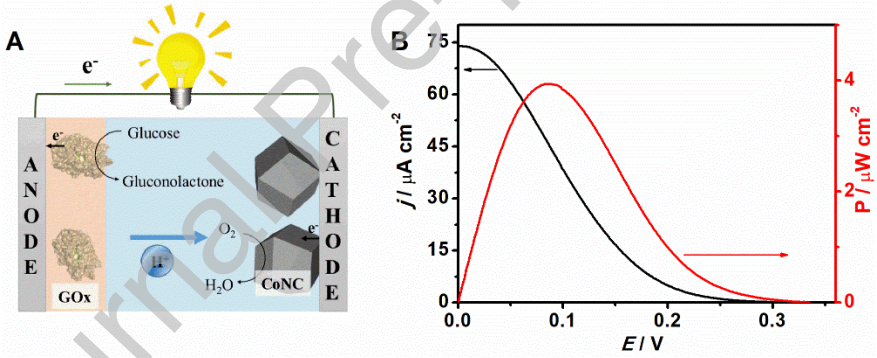

Figure 4 (A) Schematic drawing of the single-compartment hybrid EBFC with a GCE/Os(bpy)$_2$PVI/GOx bioanode and a GCE/Co-N-C-10 abiotic cathode. (B) Polarization and power density profiles of the hybrid EBFC in 0.1 M pH 7.0 PBS (air-equilibrated, 5 mM glucose).

3. Electrocatalytic ORR and stability in alkaline solution

The remarkable ORR activity of Co-N-C-10 under neutral conditions prompts us to investigate their performance in alkaline media. Co-N-C-10 catalyst shows superior ORR activity over the 20 wt% commercial Pt/C catalyst regarding to $E_{1/2}$ (0.95 and 0.94 V vs. RHE) and J_L (5.90 and 5.69 mA cm^{-2}) (**Figure 5A**). Similar to the observation in neutral electrolyte, the catalyzed ORR on Co-N-C-10 also undergoes a four-electron route according to the K-L plots, which is further validated by the low HO_2^- yield (**Figure 5B and 5C**). Furthermore, the methanol tolerance of Co-N-C-10 and commercial Pt/C was also evaluated by chronoamperometric (CA) responses experiencing the dosing of 3 M methanol. Notably, negligible interference effect upon catalytic current density is observed on the Co-N-C-10. However, Pt/C catalyst exhibits a chopped drop by ca. 25% under the similar condition (**Figure 5D**), confirming better electrocatalytic selectivity toward ORR for Co-N-C-10. Through the comparative analysis between proposed catalyst and non-precious metal containing catalysts in literature (**Table S2**), the comparable ORR performances of Co-N-C-10 suggest that it's great potential for the cathodic catalyst in alkaline fuel cells.

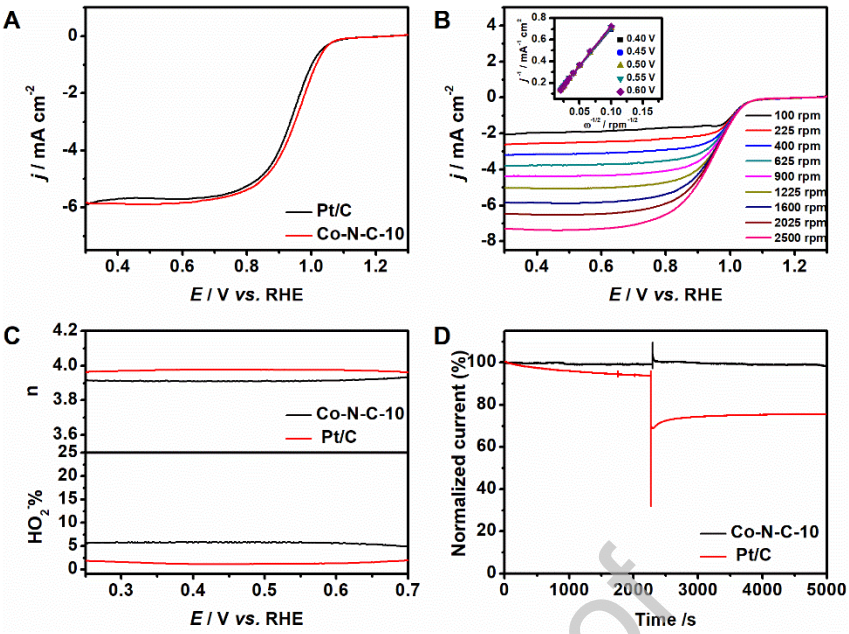

Figure 5 (A) LSVs (scan rate: 5 mV s^{-1}) of Co-N-C-10 and commercial Pt/C in O_2-saturated 0.1 M KOH solution at 1600 rpm. (B) LSV polarization curves (scan rate: 5 mV s^{-1}) of Co-N-C-10 at different rotation rates; Inset: Koutecky-Levich plots of Co-N-C-10. (C) HO_2^- yields and n of Co-N-C-10 and Pt/C derived from RRDE. (D) Amperometric profiles for Co-N-C-10 and Pt/C in O_2-saturated 0.1 M KOH solution upon the dosing of 3.0 M methanol; operation voltage: 0.5 V vs. RHE.

Conclusion

We have described a feasible method to fabricate Co and N codoped porous carbon materials based ORR electrocatalysts using one-step pyrolysis of the well-tailored Zn/Co bimetal-organic frameworks (Zn_xCo_{100-x}@ZIF). The resultant Co-N-C materials features large surface area, high porosity, suitable graphitic structure decorated with well-dispersed Co-N_x moieties. The optimal Co-N-C-10 exhibits considerable ORR activity with a positive half-wave potential, high

diffusion-limited current densities, $4e^-$ transfer pathway and superior stability, comparable to those of benchmark Pt/C in neutral solution. In addition, Co-N-C-10 also presents efficient ORR activity and outstanding methanol tolerance than Pt/C in alkaline condition. This report may hold great potential for fabrication of other transition metal and nitrogen doped carbon material toward energy conversion, such as hybrid enzymatic biofuel cells.

Credit author statement

Xiaogeng Feng: Conceptualization, Methodology, Software, Investigation, Visualization, Formal analysis, Writing-Original Draft, Writing-review&editing.
Xinxin Xiao: Conceptualization, Methodology, Visualization, Writing-review&editing, Supervision.
Jingdong Zhang: Funding acquisition.
Liping Guo: Funding acquisition, Project administration, Supervision.
Ying Xiong: Funding acquisition, Conceptualization, Project administration, Supervision

Acknowledgements

This work is supported by the financial support from National Natural Science Foundation of China (21575021, 51674131, 22006062, 51902149). X.X. acknowledges the Villum Experiment (grant No. 35844). Prof. Dónal Leech is acknowledged for kindly delivering the Os complex modified redox polymer. This article is dedicated to Professor Jens Ulstrup on the occasion of his 80th birthday.

Declaration of interests

☒ The authors declare that they have no known competing financial interests or personal relationships that could have appeared to influence the work reported in this paper.

References

[1] J. Zhang, Z. Zhao, Z. Xia, L. Dai, A metal-free bifunctional electrocatalyst for oxygen reduction and oxygen evolution reactions, Nat. Nanotechnol. 10 (2015) 444-452.

[2] S. Wang, D. Yu, L. Dai, Polyelectrolyte functionalized carbon nanotubes as efficient metal-free electrocatalysts for oxygen reduction, J. Am. Chem. Soc. 133 (2011) 5182-5185.

[3] X. Cui, S. Yang, X. Yan, J. Leng, S. Shuang, P.M. Ajayan, Z. Zhang, Pyridinic-nitrogen- Dominated graphene aerogels with Fe-N-C coordination for highly efficient oxygen reduction reaction, Adv. Funct. Mater. 26 (2016) 5708-5717.

[4] Y. Guo, P. Yuan, J. Zhang, Y. Hu, I.S. Amiinu, X. Wang, J. Zhou, H. Xia, Z. Song, Q. Xu, Carbon nanosheets containing discrete Co-N_x-B_y-C active sites for efficient oxygen electrocatalysis and rechargeable Zn-Air Batteries, ACS Nano 12 (2018) 1894-1901.

[5] F. Guo, H. Yang, B. Aguila, A.M. Al-Enizi, A. Nafady, M. Singh, V. Bansal, S. Ma, Cobalt nanoparticles incorporated into hollow doped porous carbon capsules as a highly efficient oxygen reduction electrocatalyst, Catal. Sci. Technol., 8 (2018) 5244-5250.

[6] W. Fan, Z. Li, C. You, X. Zong, X. Tian, S. Miao, T. Shu, C. Li, S. Liao, Binary Fe, Cu-doped bamboo-like carbon nanotubes as efficient catalyst for the oxygen reduction reaction, Nano Energy 37 (2017) 187-194.

[7] L. Dai, Y. Xue, L. Qu, H.-J. Choi, J.-B. Baek, Metal-free catalysts for oxygen reduction reaction, Chem. Rev. 115 (2015) 4823-4892.

[8] C. Tang, B. Wang, H.F. Wang, Q. Zhang, Defect engineering toward atomic Co-N_x-C in hierarchical graphene for rechargeable flexible solid Zn- air batteries, Adv. Mater. 29 (2017) 1703185.

[9] C.W. Bezerra, L. Zhang, K. Lee, H. Liu, A.L. Marques, E.P. Marques, H. Wang, J. Zhang, A review of Fe-N/C and Co-N/C catalysts for the oxygen reduction reaction, Electrochim. Acta 53 (2008) 4937-4951.

[10] G. Wu, A. Santandreu, W. Kellogg, S. Gupta, O. Ogoke, H. Zhang, H.-L. Wang, L. Dai, Carbon nanocomposite catalysts for oxygen reduction and evolution reactions: From nitrogen doping to transition-metal addition, Nano Energy 29 (2016) 83-110.

[11] X. Xiao, H.-q. Xia, R. Wu, L. Bai, L. Yan, E. Magner, S. Cosnier, E. Lojou, Z. Zhu, A. Liu, Tackling the challenges of enzymatic (bio) fuel cells, Chem. Rev. 119 (2019) 9509-9558.

[12] A.J. Bandodkar, J. Wang, Wearable biofuel cells: a review, Electroanalysis 28 (2016) 1188-1200.

[13] S. Cosnier, A. Le Goff, M. Holzinger, Towards glucose biofuel cells implanted in human body for powering artificial organs, Electrochem. Commun. 38 (2014) 19-23.

[14] A. Zebda, J.-P. Alcaraz, P. Vadgama, S. Shleev, S.D. Minteer, F. Boucher, P. Cinquin, D.K. Martin, Challenges for successful implantation of biofuel cells, Bioelectrochemistry 124 (2018) 57-72.

[15] N. Mano, A. de Poulpiquet, O_2 reduction in enzymatic biofuel cells, Chem. Rev.

118 (2017) 2392-2468.

[16] X. Xiao, K.D. McGourty, E. Magner, Enzymatic Biofuel Cells for Self-Powered, Controlled Drug Release, J. Am. Chem. Soc. 142 (2020) 11602-11609.

[17] X. Xiao, P.Ó. Conghaile, D. Leech, R. Ludwig, E. Magner, A symmetric supercapacitor/biofuel cell hybrid device based on enzyme-modified nanoporous gold: An autonomous pulse generator, Biosens. Bioelectron. 90 (2017) 96-102.

[18] X. Xiao, M.P. Ryan, D. Leech, J. Zhang, E. Magner, Antimicrobial enzymatic biofuel cells, Chem. Commun. 56 (2020) 15589-15592.

[19] X. Xiao, D. Leech, J. Zhang, An oxygen-reducing biocathode with "oxygen tanks", Chem. Commun. 56 (2020) 9767-9770.

[20] I. Mazurenko, X. Wang, A. De Poulpiquet, E. Lojou, H_2/O_2 enzymatic fuel cells: from proof-of-concept to powerful devices, Sustain. Energy Fuels 1 (2017) 1475-1501.

[21] C. Kang, H. Shin, A. Heller, On the stability of the "wired" bilirubin oxidase oxygen cathode in serum, Bioelectrochemistry 68 (2006) 22-26.

[22] N. Mano, H.-H. Kim, Y. Zhang, A. Heller, An oxygen cathode operating in a physiological solution, J. Am. Chem. Soc. 124 (2002) 6480-6486.

[23] V. Consonni, A.M. Lord, Polarity in ZnO nanowires: a critical issue for piezotronic and piezoelectric devices, Nano Energy (2021) 105789.

[24] L. Feng, Y. Yan, Y. Chen, L. Wang, Nitrogen-doped carbon nanotubes as efficient and durable metal-free cathodic catalysts for oxygen reduction in microbial fuel cells, Energy Environ. Sci. 4 (2011) 1892-1899.

[25] Y. Zou, J. Li, Q. Fu, L. Zhang, Q. Liao, X. Zhu, Macroporous hollow nanocarbon shell-supported Fe-N catalysts for oxygen reduction reaction in microbial fuel cellss, Electrochim. Acta 320 (2019) 134590.

[26] B. Mecheri, V.C. Ficca, M.A.C. de Oliveira, A. D'Epifanio, E. Placidi, F. Arciprete, S. Licoccia, Facile synthesis of graphene-phthalocyanine composites as oxygen reduction electrocatalysts in microbial fuel cells, Appl. Catal., B 237 (2018) 699-707.

[27] M. Kodali, C. Santoro, A. Serov, S. Kabir, K. Artyushkova, I. Matanovic, P. Atanassov, Air breathing cathodes for microbial fuel cell using Mn-, Fe-, Co-and Ni-containing platinum group metal-free catalysts, Electrochim. Acta 231 (2017) 115-124.

[28] S. Rojas-Carbonell, K. Artyushkova, A. Serov, C. Santoro, I. Matanovic, P. Atanassov, Effect of pH on the activity of platinum group metal-free catalysts in oxygen reduction reaction, ACS Catal. 8 (2018) 3041-3053.

[29] C. Santoro, A. Serov, L. Stariha, M. Kodali, J. Gordon, S. Babanova, O. Bretschger, K. Artyushkova, P. Atanassov, Iron based catalysts from novel low-cost organic precursors for enhanced oxygen reduction reaction in neutral media microbial fuel cells, Energy Environ. Sci. 9 (2016) 2346-2353.

[30] J. Li, M. Chen, D.A. Cullen, S. Hwang, M. Wang, B. Li, K. Liu, S. Karakalos, M. Lucero, H. Zhang, C. Lei, H. Xu, G.E. Sterbinsky, Z. Feng, D. Su, K.L. More, G. Wang, Z. Wang, G. Wu, Atomically dispersed manganese catalysts for oxygen reduction in proton-exchange membrane fuel cells, Nat. Catal. 1 (2018) 935-945.

[31] J.J. Perry Iv, J.A. Perman, M.J. Zaworotko, Design and synthesis of metal-organic frameworks using metal-organic polyhedra as supermolecular building blocks, Chem. Soc. Rev. 38 (2009) 1400-1417.

[32] W. Huang, J. Tang, F. Diao, C. Engelbrekt, J. Ulstrup, X. Xiao, K. Mølhave, Recent Progress of Two- Dimensional Metal- Organic Frameworks and Their Derivatives for Oxygen Evolution Electrocatalysis, ChemElectroChem 7 (2020) 4695-4712.

[33] R.R. Salunkhe, Y.V. Kaneti, J. Kim, J.H. Kim, Y. Yamauchi, Nanoarchitectures for metal-organic framework-derived nanoporous carbons toward supercapacitor applications, Acc. Chem. Res. 49 (2016) 2796-2806.

[34] V. Armel, S. Hindocha, F. Salles, S. Bennett, D. Jones, F.d.r. Jaouen, Structural descriptors of zeolitic-imidazolate frameworks are keys to the activity of Fe-N-C catalysts, J. Am. Chem. Soc. 139 (2017) 453-464.

[35] W. Zhang, Z.-Y. Wu, H.-L. Jiang, S.-H. Yu, Nanowire-directed templating synthesis of metal-organic framework nanofibers and their derived porous doped carbon nanofibers for enhanced electrocatalysis, J. Am. Chem. Soc. 136 (2014) 14385-14388.

[36] L. Chai, L. Zhang, X. Wang, L. Xu, C. Han, T.-T. Li, Y. Hu, J. Qian, S. Huang, Bottom-up synthesis of MOF-derived hollow N-doped carbon materials for enhanced ORR performance, Carbon 146 (2019) 248-256.

[37] Z. Li, M. Shao, L. Zhou, R. Zhang, C. Zhang, M. Wei, D.G. Evans, X. Duan, Directed Growth of Metal- Organic Frameworks and Their Derived Carbon- Based

Network for Efficient Electrocatalytic Oxygen Reduction, Adv. Mater. 28 (2016) 2337-2344.

[38] B.Y. Guan, L. Yu, X.W. Lou, Formation of single- holed cobalt/N- doped carbon hollow particles with enhanced electrocatalytic activity toward oxygen reduction reaction in alkaline media, Adv. Sci. 4 (2017) 1700247.

[39] Y.Z. Chen, C. Wang, Z.Y. Wu, Y. Xiong, Q. Xu, S.H. Yu, H.L. Jiang, From Bimetallic Metal-Organic Framework to Porous Carbon: High Surface Area and Multicomponent Active Dopants for Excellent Electrocatalysis, Adv. Mater. 27 (2015) 5010-5016.

[40] J. Qian, F. Sun, L. Qin, Hydrothermal synthesis of zeolitic imidazolate framework-67 (ZIF-67) nanocrystals, Mater. Lett. 82 (2012) 220-223.

[41] J.B. Allen, R.F. Larry, Electrochemical methods fundamentals and applications, John Wiley & Sons 2001.

[42] J.I. Jung, H.Y. Jeong, J.S. Lee, M.G. Kim, J. Cho, A bifunctional perovskite catalyst for oxygen reduction and evolution, Angew. Chem. Int. Ed. 126 (2014) 4670-4674.

[43] X. Xiao, E. Magner, A biofuel cell in non-aqueous solution, Chem. Commun. 51 (2015) 13478-13480.

[44] X. Xiao, E. Magner, A quasi-solid-state and self-powered biosupercapacitor based on flexible nanoporous gold electrodes, Chem. Commun. 54 (2018) 5823-5826.

[45] W. Shao, C. He, M. Zhou, C. Yang, Y. Gao, S. Li, L. Ma, L. Qiu, C. Cheng, C. Zhao, Core-shell-structured MOF-derived 2D hierarchical nanocatalysts with

enhanced Fenton-like activities, J. Mater. Chem. A. 8 (2020) 3168-3179.

[46] S. Zhao, H. Yin, L. Du, L. He, K. Zhao, L. Chang, G. Yin, H. Zhao, S. Liu, Z. Tang, Carbonized nanoscale metal-organic frameworks as high performance electrocatalyst for oxygen reduction reaction, ACS Nano 8 (2014) 12660-12668.

[47] Y. Hou, Z. Wen, S. Cui, S. Ci, S. Mao, J. Chen, An advanced nitrogen- doped graphene/cobalt- embedded porous carbon polyhedron hybrid for efficient catalysis of oxygen reduction and water splitting, Adv. Funct. Mater. 25 (2015) 872-882.

[48] J.-C. Li, X.-T. Wu, L.-J. Chen, N. Li, Z.-Q. Liu, Bifunctional MOF-derived Co-N-doped carbon electrocatalysts for high-performance zinc-air batteries and MFCs, Energy, 156 (2018) 95-102.

[49] C. Liu, J. Wang, J. Li, J. Liu, C. Wang, X. Sun, J. Shen, W. Han, L. Wang, Electrospun ZIF-based hierarchical carbon fiber as an efficient electrocatalyst for the oxygen reduction reaction, J. Mater. Chem. A. 5 (2017) 1211-1220.

[50] X. Feng, X. Bo, L. Guo, CoM(M=Fe,Cu,Ni)-embedded nitrogen-enriched porous carbon framework for efficient oxygen and hydrogen evolution reactions, J. Power Sources 389 (2018) 249-259.

[51] A. Christenson, S. Shleev, N. Mano, A. Heller, L. Gorton, Redox potentials of the blue copper sites of bilirubin oxidases, BBA-Bioenergetics 1757 (2006) 1634-1641.

[52] S. Zheng, X. Li, B. Yan, Q. Hu, Y. Xu, X. Xiao, H. Xue, H. Pang, Transition-metal (Fe, Co, Ni) based metal- organic frameworks for electrochemical energy storage, Adv. Energy Mater. 7 (2017) 1602733.

[53] H. Park, S. Oh, S. Lee, S. Choi, M. Oh, Cobalt- and nitrogen-codoped porous

carbon catalyst made from core-shell type hybrid metal-organic framework (ZIF-L@ZIF-67) and its efficient oxygen reduction reaction (ORR) activity, Appl. Catal., B 246 (2019) 322-329.

[54] J. Su, G. Xia, R. Li, Y. Yang, J. Chen, R. Shi, P. Jiang, Q. Chen, Co_3ZnC/Co nano heterojunctions encapsulated in N-doped graphene layers derived from PBAs as highly efficient bi-functional OER and ORR electrocatalysts, J. Mater. Chem. A. 4 (2016) 9204-9212.

[55] M. Zhang, L. Dai, Carbon nanomaterials as metal-free catalysts in next generation fuel cells, Nano Energy 1 (2012) 514-517.

[56] B.Y. Xia, Y. Yan, N. Li, H.B. Wu, X.W. Lou, X. Wang, A metal-organic framework-derived bifunctional oxygen electrocatalyst, Nat. Energy 1 (2016) 15006.

[57] J.-N. Zhang, S.-J. You, Y.-X. Yuan, Q.-L. Zhao, G.-D. Zhang, Efficient electrocatalysis of cathodic oxygen reduction with Pt-Fe alloy catalyst in microbial fuel cell, Electrochem. Commun. 13 (2011) 903-905.

[58] Z. Wang, C. Cao, Y. Zheng, S. Chen, F. Zhao, Abiotic oxygen reduction reaction catalysts used in microbial fuel cells, ChemElectroChem 1 (2014) 1813-1821.

[59] I. Mazurenko, K. Monsalve, P. Infossi, M.-T. Giudici-Orticoni, F. Topin, N. Mano, E. Lojou, Impact of substrate diffusion and enzyme distribution in 3D-porous electrodes: a combined electrochemical and modelling study of a thermostable H_2/O_2 enzymatic fuel cell, Energy Environ. Sci. 10 (2017) 1966-1982.

[60] A. Gross, M. Holzinger, S. Cosnier, Buckypaper bioelectrodes: Emerging materials for implantable and wearable biofuel cells, Energy Environ. Sci. 11 (2018) 1670-1687.